The Effects of Evaporation on Frontal Circulations

HO-CHUN HUANG AND KERRY A. EMANUEL

Center for Meteorology and Physical Oceanography, Massachusetts Institute of Technology, Cambridge, Massachusetts

(Manuscript received 3 April 1990, in final form 2 October 1990)

ABSTRACT

The condensation of water vapor in the ascent region of frontal zones has been shown by many studies to increase substantially the rate of frontogenesis. Phase change of water substance in the downdraft has, however, received comparatively little attention. Here we add evaporation of falling rain to a semigeostrophic model of frontogenesis that also allows for condensation heating in the updraft, as in previous work. Evaporation of rain significantly increases the rate of frontogenesis and, more dramatically, leads to a strong, concentrated sloping downdraft just beneath the narrow sheet of saturated ascent.

1. Introduction

The last two decades have witnessed significant advances in the understanding of fronts and frontogenesis, due principally to the advent of semigeostrophic theory (Hoskins 1971; Hoskins and Bretherton 1972) and to detailed mesoscale field programs. The main features of surface frontogenesis, including the collapse to a discontinuity in a finite, realistic time and the structure of the wind and pressure fields have been successfully explained. Upper fronts have proven more difficult to deal with, but here too there has been significant progress (Keyser and Shapiro 1986). Recent integrations of Lagrangian-coordinate primitive equation models (Garner 1989) verify the integrity of the semigeostrophic equations applied to frontogenesis in nearly inviscid, slow deformation fields.

In recent years there has also been notable progress in understanding the effects of nonconservative processes on fronts and frontogenesis. The action of surface friction and boundary layer turbulence in frontal zones has been examined by Keyser and Anthes (1982), and the substantial influence of condensation of water vapor on frontal characteristics has been investigated by Hsie et al. (1984), Thorpe and Nash (1984), Williams et al. (1981), Emanuel (1985), and Thorpe and Emanuel (1985), among others. The last-mentioned authors made use of recent field experimental data that shows that the ascent regions of many frontal zones are nearly neutral to slantwise moist convection. When this condition is explicitly incorporated in a semigeostrophic frontogenesis model, the frontogenesis proceeds somewhat more rapidly than in the dry case, and the updraft collapses onto a thin, rapidly ascending sheet. Examination of frontogenesis in the context of developing baroclinic waves under moist neutral conditions (Emanuel et al. 1987) confirms these features of moist frontogenesis and shows that baroclinic instability develops almost twice as quickly under moist neutral as under dry conditions.

When condensed water falls out of the gently sloping frontal updraft, it generally falls through the colder, drier descending air on the cold side of the frontal zone. Some of it may be expected to evaporate and, if it begins in frozen form and passes through a melting level, some or all of it may melt. There is considerable evidence that evaporation of rain has significant effects on the evolution of fronts. Perhaps the first detailed analysis of such effects is that of Oliver and Holzworth (1953), who proposed that the rapid cooling by evaporation may lead to rapid surges in the advance of surface cold fronts. The generation of mesoscale circulations by melting snow has been examined extensively by Carbone (1982), Atlas et al. (1969), Stewart (1985), and Szeto et al. (1988a,b), among others. It appears that such circulations may have noticeable amplitude.

The purpose of the present work is to attempt to treat the evaporation of rain as part of an entire frontogenesis process and to explicitly examine the effects of evaporation on the frontal circulations. We do so in the framework of a moist semigeostrophic model under the assumption that evaporative cooling is not so strong as to invalidate the geostrophic momentum approximation, an assumption that we validate a posteriori.

The semigeostrophic model is described in the following section, while results of the model integration are presented in section 3. A summary of this work appears in section 4.

Corresponding author address: Dr. Kerry A. Emanuel, Center for Meteorology and Physical Oceanography, MIT, Cambridge, MA 02139.

2. Semigeostrophic numerical model

The two-dimensional, moist semigeostrophic frontal model of Thorpe and Emanuel (1985) is used as the basis of the present work. This model integrates the dimensionless form of the moist semigeostrophic equations for the development of a two-dimensional front in a background of constant geostrophic stretching deformation, with initially constant interior potential vorticity. (Due to phase changes of water, the potential vorticity does not remain constant but develops a highly concentrated positive anomaly in the surface frontal zone and a diffuse negative anomaly in the upper troposphere.) The dynamics of the frontal development are controlled by the initial distribution of temperature on the boundaries and by a single dimensionless parameter γ:

$$\gamma \equiv \frac{\Gamma_m}{\Gamma_d}\frac{q_{ge}}{q_{go}},$$

where Γ_m and Γ_d are average values of the moist and dry adiabatic lapse rates, respectively, and q_{ge} and q_{go} are the equivalent potential vorticity and initial (dry) potential vorticity, respectively. (The equivalent potential vorticity is simply the dot product of the absolute vorticity and the gradient of equivalent potential temperature. It is conserved in two-dimensional flow in the absence of heating other than latent heating, and of friction.) The parameter γ is the ratio of the moist to the dry slantwise stability and is assumed to be small, as indicated by the observations of Emanuel (1988). The initial state is assumed to be just saturated but to contain no liquid water.

Emanuel (1985), Thorpe and Emanuel (1985), and Emanuel, Fantini and Thorpe (1987) implicitly neglect the effect of evaporation of raindrops by assuming that once the raindrop is formed it will fall and reach the ground in a time short enough that no evaporation will take place. This assumption may be reasonable for raindrops formed in the lower portion of the atmosphere. But the depth of the atmosphere that is used in these studies is about 10 km. Thus, precipitation may fall through deep unsaturated regions of the atmosphere, affecting temperatures over a large volume through evaporation. The inclusion of the effects of evaporation should be important in understanding the dynamical structure of baroclinic waves and frontogenesis. After reviewing the system of Thorpe and Emanuel (1985), we add equations governing the fall and evaporation of raindrops.

a. *Review of the moist semigeostrophic frontogenesis model*

The model is phrased in geostrophic coordinates, as defined by Hoskins and Bretherton (1972). For a north–south frontal zone in the Northern Hemisphere, they are

$$X = x + \frac{v_g}{f}$$

$$Z = z$$

$$\tau = t,$$

where v_g is the geostrophic flow in the along-front (northward) direction, f is the Coriolis parameter, and z is a "pseudoheight" defined by

$$z = \left[1 - \left(\frac{p}{p_0}\right)^{\kappa}\right]\frac{H_s}{\kappa},$$

in which $H_s \equiv p_0/\rho_0 g$, $\kappa \equiv R/c_p$, ρ is the density, g the acceleration of gravity, R the gas constant of dry air, c_p the heat capacity at constant pressure of dry air, and the subscript zero denotes a typical surface reference value. To a good approximation, z can be treated as physical altitude in the troposphere.

The governing semigeostrophic equations consist of a time-dependent potential vorticity equation, the definition of potential vorticity in the semigeostrophic system, and a diagnostic equation for the ageostrophic streamfunction in the X–Z plane:

$$\frac{dq}{d\tau} = \frac{\zeta}{\rho}\frac{\partial S}{\partial Z} \tag{1}$$

$$\frac{\partial^2\Phi}{\partial X^2} + \frac{f^3\theta_0}{q\rho g}\frac{\partial^2\Phi}{\partial Z^2} = f^2 \tag{2}$$

$$\rho\frac{\partial}{\partial Z}\left(\frac{1}{\rho}\frac{\partial\psi}{\partial Z}\right) + \frac{\partial}{\partial X}\left(q\frac{\rho g}{f^3\theta_0}\frac{\partial\psi}{\partial X}\right) = -2Q - \frac{\rho g}{f^2\theta_0}\frac{\partial S}{\partial X}. \tag{3}$$

Here, q is the potential vorticity, which is related to potential temperature θ and absolute vorticity ζ by

$$q = \frac{\zeta}{\rho}\frac{\partial\theta}{\partial Z}, \tag{4}$$

S is the heating:

$$S \equiv \frac{d\theta}{d\tau}, \tag{5}$$

Q is the geostrophic forcing by the background deformation flow:

$$Q \equiv \rho\frac{\alpha}{f}\frac{\partial V_g}{\partial Z}, \tag{6}$$

where α is half the magnitude of the deformation; Φ is a modified geopotential:

$$\Phi \equiv \phi + \frac{1}{2}v_g^2,$$

where ϕ is the actual geopotential; and ψ is an ageostrophic streamfunction such that

$$\rho u_a \equiv \frac{\partial \psi}{\partial z},$$

$$\rho w \equiv -\frac{\partial \psi}{\partial x},$$

where u_a and w are the ageostrophic cross-front wind and vertical velocity, respectively.

The boundary conditions consist of rigid surfaces at the earth's surface and at a specified height Z_{top}. At these boundaries we require that $\psi = 0$, so that the thermodynamic equation at the boundaries has the form

$$\left(\frac{\partial}{\partial \tau} - \alpha X \frac{\partial}{\partial X}\right)\frac{\partial \Phi}{\partial Z} = \frac{Sg}{\theta_0} \quad \text{on} \quad Z = 0, Z_{\text{top}}. \tag{7}$$

This provides the necessary boundary condition used in inverting (2) for Φ. (In Thorpe and Emanuel 1985, S is always zero on the boundaries but may be nonzero in the present case because rain may evaporate at the surface.)

The total time derivative that appears in (1) is expanded in geostrophic coordinates, and after accounting for the background deformation flow, has the form

$$\frac{d}{d\tau} = \frac{\partial}{\partial \tau} - \alpha X \frac{\partial}{\partial X} - \frac{\zeta}{f}\frac{\partial \psi}{\partial X}\frac{\partial}{\partial Z}. \tag{8}$$

Given the heating S, the system (1)–(3) together with (7) is solved as follows: First, the potential vorticity equation (1) is integrated forward in time, using (8) to expand the Lagrangian time derivative, and (7) is advanced as well. Then (2) and (3) are inverted to find the new values of ψ and Φ. The geostrophic wind and potential temperature may then be diagnosed from the geostrophic and hydrostatic relationships:

$$f v_g = \frac{\partial \Phi}{\partial X},$$

$$\frac{g}{\theta_0}\theta = \frac{\partial \Phi}{\partial Z}.$$

Following Thorpe and Emanuel (1985), the heating in the regions where water is condensed is dictated by the requirement that moist entropy (equivalent potential temperature) is conserved. They showed that such a heating may be related to vertical velocity by

$$S \approx \begin{cases} \dfrac{w}{\zeta}\left(q - \dfrac{\Gamma_m}{\Gamma_d} q_e\right), & \text{for} \quad w > 0 \\ 0, & \text{for} \quad w \leqslant 0, \end{cases} \tag{9}$$

where q_e is the equivalent potential vorticity. As we take q_e to be very small, we ignore the variation of Γ_m/Γ_d through the depth of the troposphere. (This involves a small correction to the formulation of Thorpe and Emanuel 1985, who omitted the factor Γ_m/Γ_d.)

As it will be necessary to keep track of water substance in the present case, we integrate an equation for water vapor mixing ratio. Where water vapor is condensing this has the form

$$\frac{dr_v}{d\tau} = -\frac{C_p \Pi}{L_v} S \quad \text{for} \quad r_v = r_{vs}, \tag{10}$$

where r_v and r_{vs} are the actual and saturation mixing ratios, respectively; L_v is the heat of vaporization and

$$\Pi \equiv \left(\frac{p}{p_0}\right)^{\kappa}.$$

b. Conservation of water and evaporative cooling

The new feature of the present model is cooling due to evaporation of rain. In regions where rain is evaporating, the heating is given by

$$S = -\frac{L_v}{C_p \Pi} E_r, \tag{11}$$

where E_r is the rate of evaporation of rain. In order to determine this, it is necessary to find the rainwater content. For this purpose *we assume that all condensed water is in the form of rain* and integrate a conservation equation for rain water of the form (in physical coordinates)

$$\frac{dr_l}{dt} - \frac{1}{\bar{\rho}}\frac{\partial}{\partial z}(\bar{\rho} V_T r_l) = \begin{cases} -\dfrac{dr_v}{dt}, & w \geqslant 0 \\ -E_r, & w < 0, \end{cases} \tag{12}$$

where V_T is the terminal velocity of rain and $\bar{\rho}$ is a horizontally averaged density. Here r_l is the rainwater mixing ratio. After transformation to geostrophic coordinates, (12) becomes

$$\frac{dr_l}{d\tau} - \left[\frac{\zeta}{\bar{\rho} f^2}\frac{\partial v_g}{\partial Z}\frac{\partial}{\partial X} + \frac{1}{\bar{\rho}}\frac{\partial}{\partial Z}\right](\bar{\rho} V_T r_l) = \begin{cases} -\dfrac{dr_v}{dt}, & w \geqslant 0 \\ -E_r, & w < 0. \end{cases} \tag{13}$$

In solving (13) we apply the boundary condition

$$r_l = 0 \quad \text{at} \quad Z_1 = Z_{\text{top}},$$

i.e., no rain falls into the model domain from above.

One technical problem that arises in solving (13) concerns the first term in brackets. This advection term becomes very large in the frontal zone where both ζ and $\partial v_g/\partial Z$ are large. This is a consequence of the fact that rain falls downward with respect to the air in physical space, not in geostrophic space, and may therefore cut across geostrophic coordinate surfaces at an extraordinary rate. This advection term therefore requires special treatment, as discussed later.

In the descent region, conservation of water vapor requires that

$$\frac{dr_v}{d\tau} = E_r. \tag{14}$$

The rate of evaporation of rainwater and its terminal velocity, as well as the saturation mixing ratio are similar to those used by Klemp and Wilhelmson (1978). They are

$$E_r = \begin{cases} \dfrac{1}{\bar{\rho}} \dfrac{(1 - r_v/r_{vs})C(\bar{\rho} r_l)^{0.525}}{5.4 \times 10^5 + 2.55 \times 10^6/\bar{p} r_{vs}}, & \text{RH} < 1.0 \\ 0, & \text{RH} = 1.0 \end{cases} \tag{15}$$

where

$$C = 1.6 + 124.9(\bar{\rho} r_l)^{0.2046} \tag{16}$$

$$r_{vs} = \frac{3.8}{\bar{p}} \exp\left(17.27 \frac{T - 273}{T - 36}\right). \tag{17}$$

The terminal velocity V_T is

$$V_T = 36.34(\bar{\rho} r_l)^{0.1364}\left(\frac{\bar{\rho}}{\rho_0}\right)^{-0.5} \quad (\text{m s}^{-1}). \tag{18}$$

The unit of $\bar{\rho}$ in (15), (16), and (18) is g cm^{-3}, and the unit of pressure in (15) and (17) is mb.

Condensation and evaporation very much alter the scales of frontal circulations and so require a reassessment of the validity of the geostrophic momentum approximation. This was done for the moist case without evaporation by Emanuel (1985), who showed that the ratio of moist to dry potential vorticity must not be too small; the solutions presented in that paper and in the present work for very small moist potential vorticity press the limits of validity of the equations. In the Appendix we present a scale analysis of the magnitude of the ageostrophic accelerations produced by the evaporation of rain.

c. *Numerical scheme and initial conditions*

A leap-frog time differencing scheme is employed, with a Euler scheme applied every 5 time steps to damp the computational mode. A simple relaxation method is used to solve the elliptic equations. The equations are integrated over a domain of 2400 km × 10 km, with a grid spacing of 40 km in X and 250 m in Z, while the time step is 60 s for Expt. D and Expt. C and 20 s for Expt. E. A smaller time step of 1 s is used to integrate the liquid water equation (13) for the reasons stated earlier. Even so, the liquid water field becomes noisy very close to the time of frontal collapse due to the very large magnitude of the advecting term, which is proportional to vorticity. Experiments with the model reveal, however, that this noise does not seem to affect the pressure fields. This is only a problem very close to the time of frontal collapse.

The model is initialized with constant potential vorticity, q_{g0}. This remains constant in the dry model, but changes due to both condensation and evaporation in the present model. In the moist case, it is difficult to begin with a balanced moist circulation because no simple analytical approximation to this exists. Thus we begin the moist simulations with a dry initial condition ($\gamma = 1$) and gradually decrease γ to the value 0.07 during the first hour. It is thereafter held fixed.

The initial temperature distribution on the lower boundary is an inverse tangent profile, as in previous studies. It has the form

$$\Phi_Z = \frac{g}{\theta_0} \frac{2\Delta\theta}{\pi} \tan^{-1}\left(\frac{X}{L}\right), \tag{19}$$

where $\Delta\theta$ is the total horizontal potential temperature difference across the domain and L governs the scale of variation of θ.

The constancy of potential vorticity in the initial condition dictates that at $t = 0$

$$\Phi_Z = \frac{g}{\theta_0}\left[\frac{2\Delta\theta}{\pi} \tan^{-1}\left(\frac{X}{L}\right) + \frac{\rho q_0 Z_{\text{top}}}{f}\right] \tag{20}$$

on the top boundary,

$$\Phi = g\frac{\Delta\theta}{\theta_0}\left(Z - \frac{H}{2}\right) + \frac{\rho g q_0}{\theta_0 f}\frac{Z^2}{2}, \tag{21}$$

on the right lateral boundary, and

$$\Phi = -g\frac{\Delta\theta}{\theta_0}\left(Z - \frac{H}{2}\right) + \frac{\rho g q_0}{\theta_0 f}\frac{Z^2}{2} \tag{22}$$

on the left lateral boundary.

As there are no diabatic effects permitted on the top boundary, the temperature distribution there will be given by (20) with L replaced by

$$L_0 \exp(-\alpha\tau).$$

No diabatic effects are permitted at the lateral boundaries.

The initial values of L, q, and $\Delta\theta$ are

$$L_0 = 380 \text{ km},$$

$$q_0 = 2.67 \times 10^{-7} \text{ m}^2 \text{ s}^{-1} \text{ K kg}^{-1},$$

$$\Delta\theta = 10 \text{ K}.$$

A constant geostrophic deformation rate, α, of 10^{-5} s^{-1} is used, and the reference values at the surface are

$$p_0 = 1000 \text{ mb},$$

$$\theta_0 = 288 \text{ K},$$

$$\rho_0 = 1.2 \text{ kg m}^{-3}.$$

The initial flow is taken to be saturated everywhere that there is upward motion, with a relative humidity of 70% elsewhere. This ensures that evaporation of falling rain occurs early on.

TABLE 1. Maximum and minimum values of various quantities for the three cases, and time to frontal collapse.

	D (24 hours)		C (24 hours)		E (22 hours)	
	max	min	max	min	max	min
v_g (m s^{-1})	36.17	−36.17	39.52	−39.51	37.73	−43.24
ζ (10^{-4} s^{-1})						
Upper boundary	3.10	0.58	4.00	0.51	3.13	0.53
Lower boundary	3.10	0.58	12.52	0.56	20.97	0.35
w (cm s^{-1})	1.04	−1.04	3.39	−1.38	3.04	−1.52
u_a (m s^{-1})	5.14	−5.14	6.27	−6.28	7.08	−5.94
q (10^{-7} kg^{-1} m^2 K s^{-1})	—	—	19.30	1.77	13.79	1.87
Time to frontal collapse (hours)	33.43		25.77		22.92	

3. Results

We report the results of three different experiments designed to examine the sensitivity of frontogenesis to evaporation of rain. The first, Expt. D, has no phase changes of water and thus reproduces the results of Hoskins and Bretherton (1972). The second, Expt. C, allows for condensation in the updraft but not evaporation; it is identical to the moist frontogenesis simulation of Thorpe and Emanuel (1985). Expt. E includes the evaporation of rain as well as condensation.

The results of three experiments are summarized in Table 1, which lists the maximum and minimum values of, respectively, the along-front velocity (v_g), vertical component of absolute vorticity (ζ), vertical velocity (w), cross-front velocity (u), and potential vorticity (q). These are listed at 24 hours, for cases D and C, and 22 hours in case E.

The dry case (Expt. D) has been discussed extensively by Hoskins and Bretherton (1972), and many others and will not be dwelt upon here, except to note that the circulation is symmetric in the sense that minima and maxima of the various quantities have the same magnitude. Likewise, the moist case with no evaporation (Expt. C) has been dealt with by Thorpe and Emanuel (1985). Here, while the magnitudes of the cross-front and long-front velocities remain almost precisely symmetric, the vorticity, potential vorticity and vertical velocities develop powerful asymmetries by 24 hours. The magnitude of the entire frontogenesis

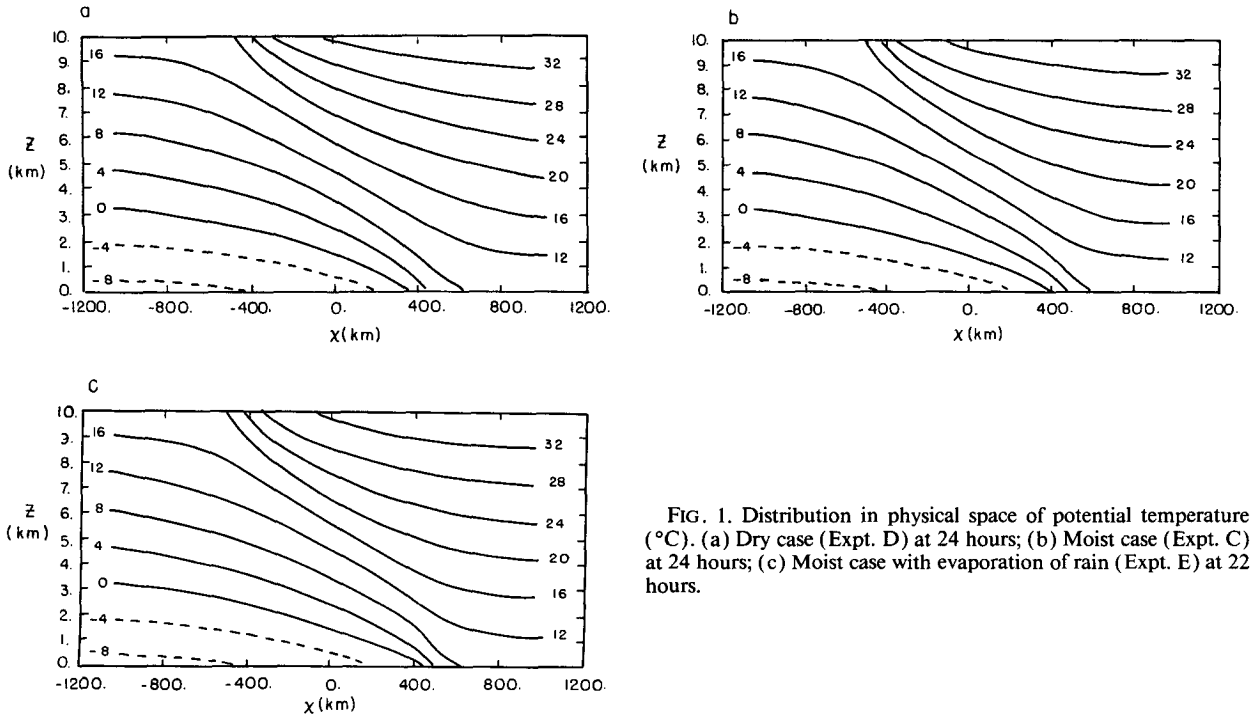

FIG. 1. Distribution in physical space of potential temperature (°C). (a) Dry case (Expt. D) at 24 hours; (b) Moist case (Expt. C) at 24 hours; (c) Moist case with evaporation of rain (Expt. E) at 22 hours.

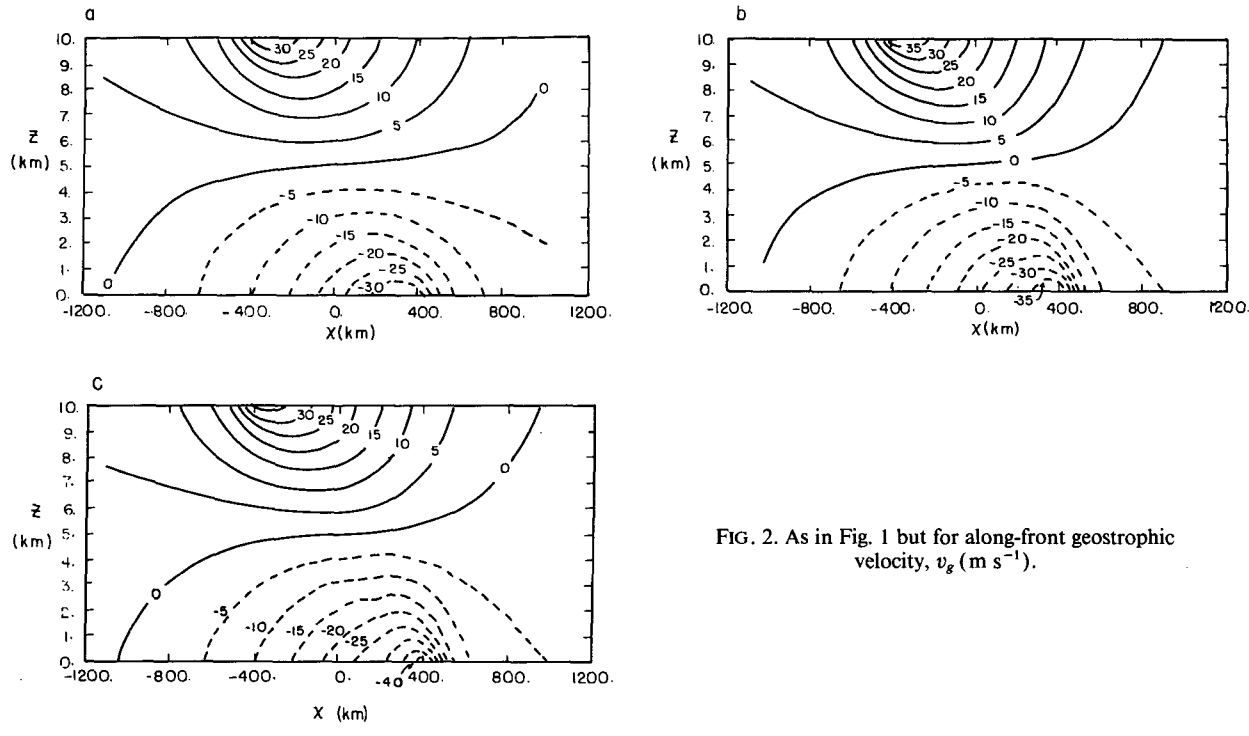

FIG. 2. As in Fig. 1 but for along-front geostrophic velocity, v_g (m s^{-1}).

is enhanced, and frontal collapse occurs at the lower boundary at 25.77 hours, in comparison to the dry case, for which frontal collapse occurs simultaneously at both boundaries at 33.43 hours.

The effects of rain evaporation are reflected in all the fields listed in Table 1. In contrast to the previous experiments, evaporation causes a noticeable asymmetry in the horizontal velocity magnitudes, with stronger flow of cold air toward the front along the surface. The circulation is slightly stronger than in the

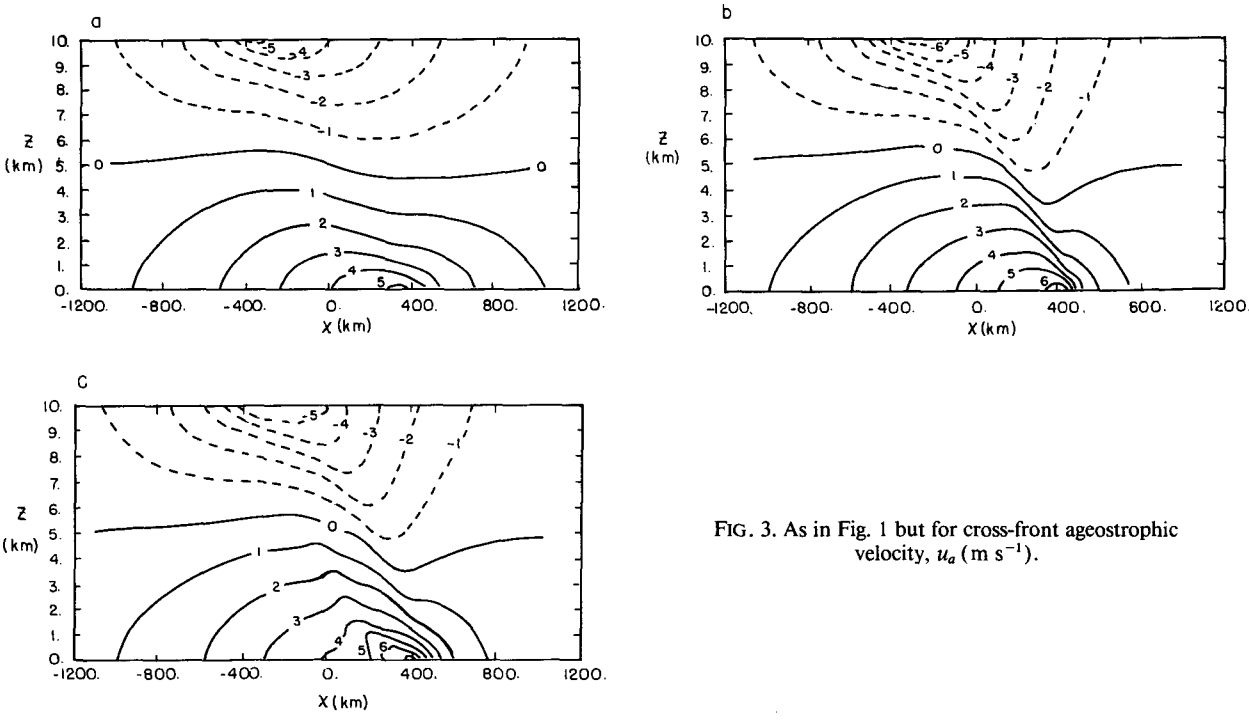

FIG. 3. As in Fig. 1 but for cross-front ageostrophic velocity, u_a (m s^{-1}).

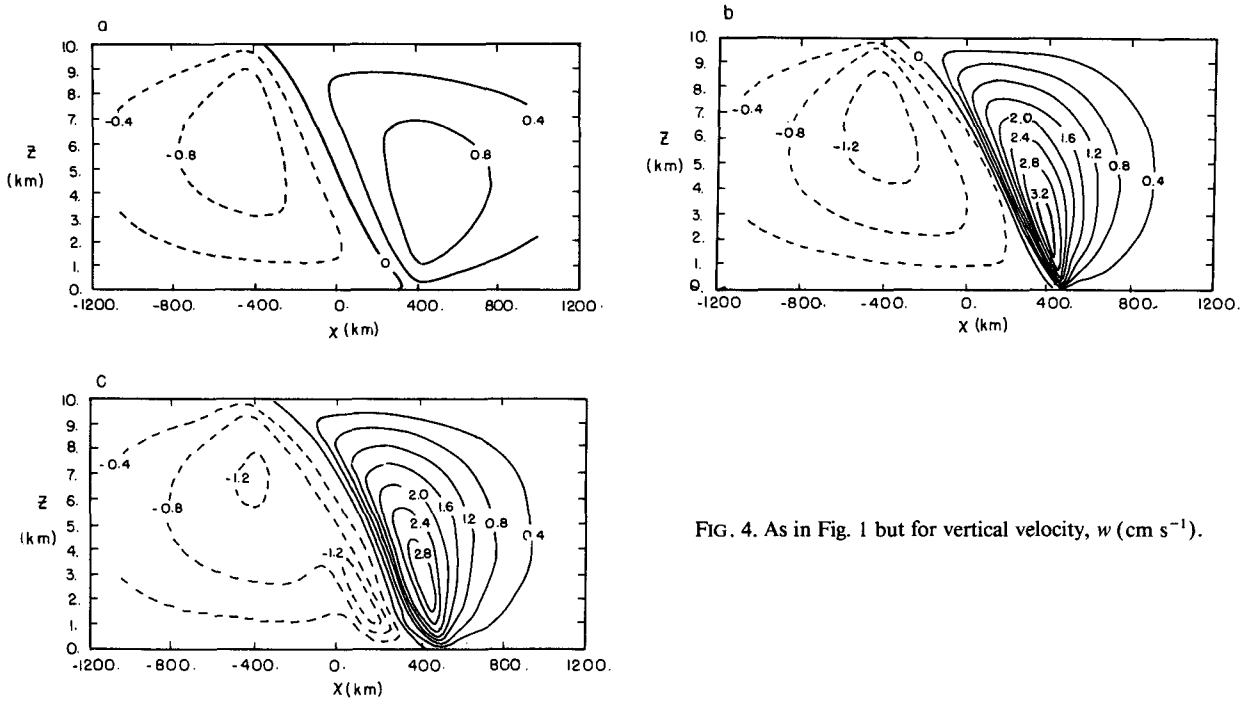

FIG. 4. As in Fig. 1 but for vertical velocity, w (cm s^{-1}).

condensation-only case (Expt. C), with frontal collapse occurring at 22.92 hours. The magnitudes of the various fields near the top boundary are hardly affected by evaporation, while, as may be expected, the downdraft is proportionally strengthened. It is almost half as strong as the updraft.

Of perhaps more interest are the fields of potential temperature, along-front velocity, cross-front velocity, vertical velocity, ageostrophic streamfunction, vorticity, and potential vorticity, which are shown at 24 hours in Figs. 1–7, respectively. All the figures show distributions in physical space. (Fields in Expt. E are shown

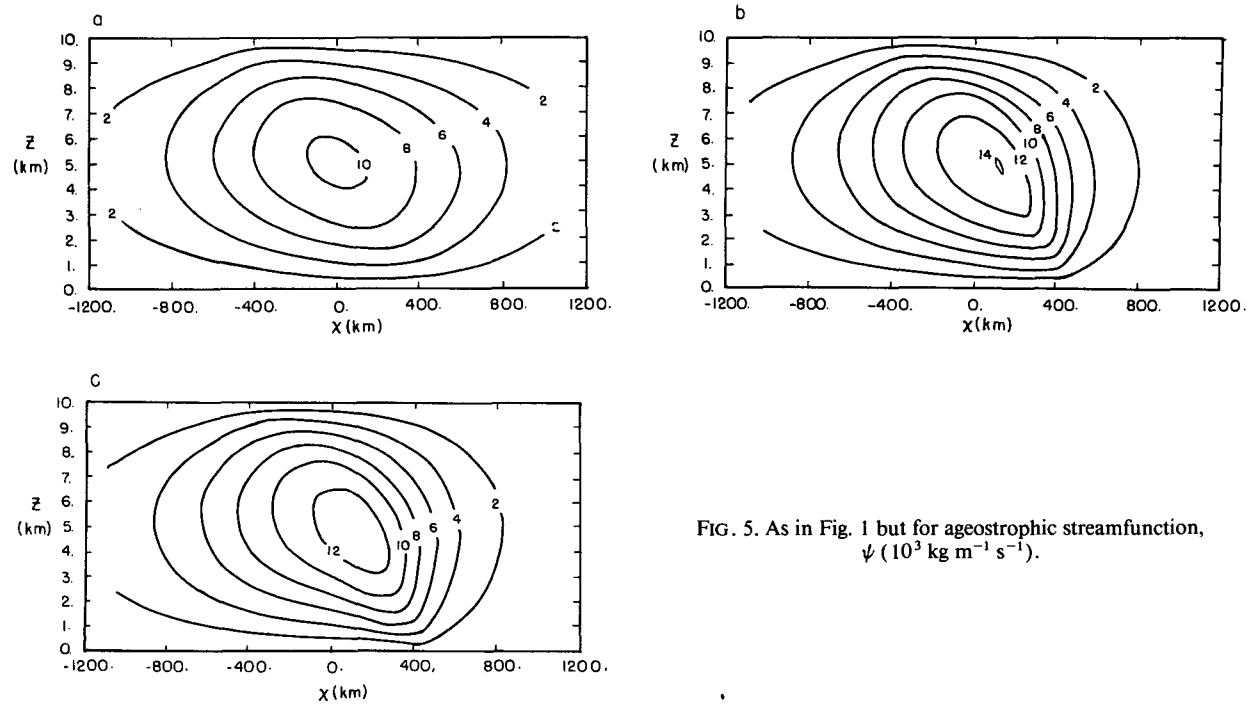

FIG. 5. As in Fig. 1 but for ageostrophic streamfunction, ψ (10^3 kg m^{-1} s^{-1}).

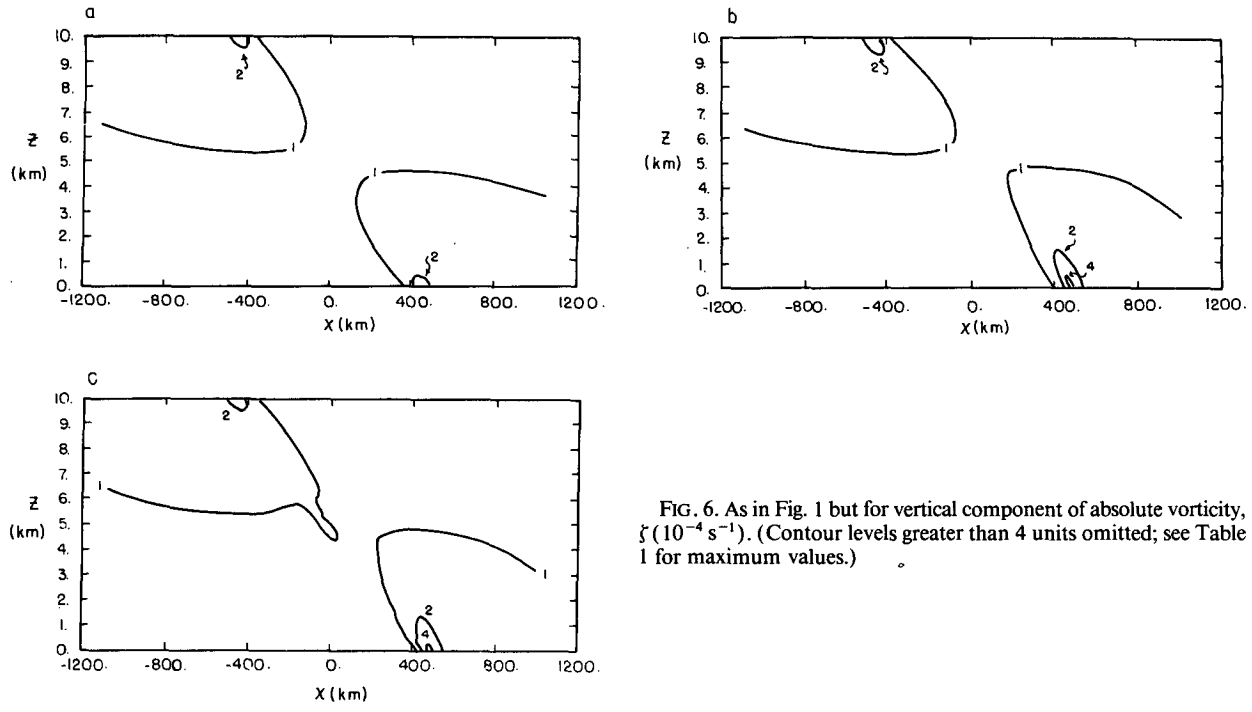

FIG. 6. As in Fig. 1 but for vertical component of absolute vorticity, ζ (10^{-4} s^{-1}). (Contour levels greater than 4 units omitted; see Table 1 for maximum values.)

at 22 hours.) Figure 8 shows the rain water distribution in Expt. E at 22 hours. The most striking effect of evaporation is seen in the cross-front and vertical velocity fields (Figs. 3 and 4), which, taken together, reveal a strong, concentrated downdraft just on the cold side of the frontal zone, to complement the sloping warm updraft on the ascent side noted by Thorpe and Emanuel (1985) and Emanuel et al. (1987). This concentrated downdraft, which is absent in the condensation-only case (Expt. C), occurs on the back side of the rainy area (Fig. 8) and is driven by the evaporation of rain. Note from Fig. 4 that the slope of the updraft–

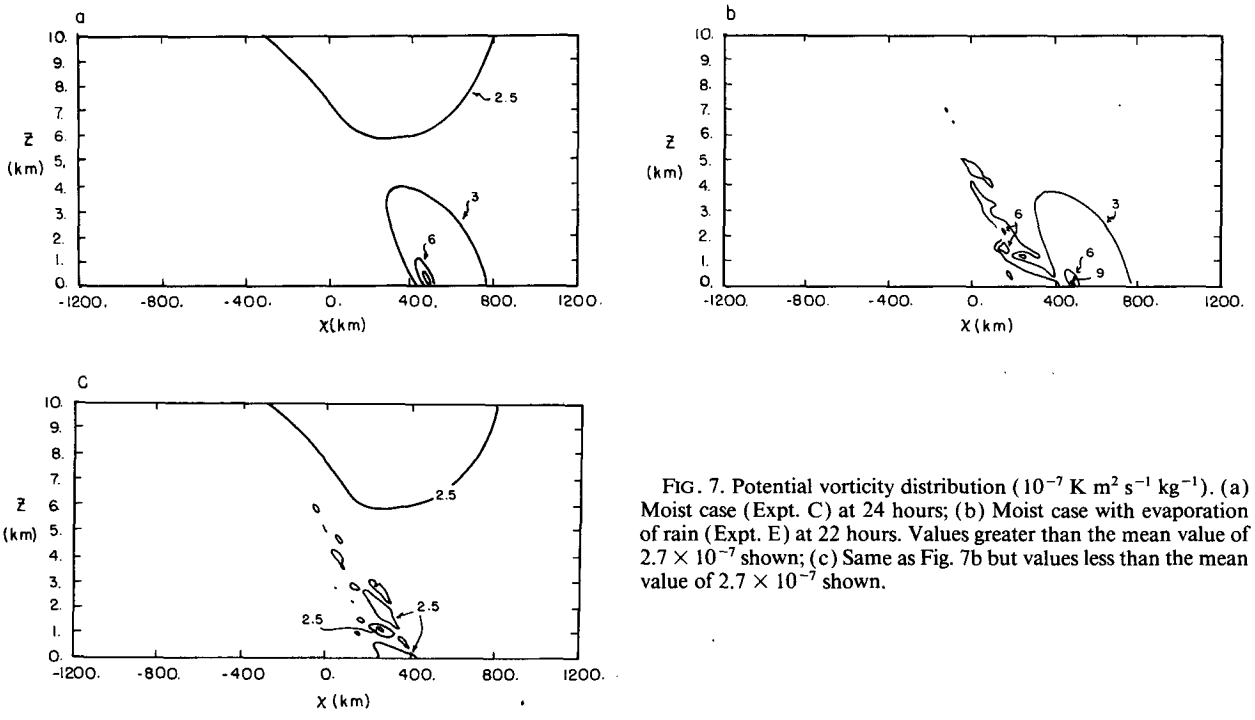

FIG. 7. Potential vorticity distribution (10^{-7} K m^2 s^{-1} kg^{-1}). (a) Moist case (Expt. C) at 24 hours; (b) Moist case with evaporation of rain (Expt. E) at 22 hours. Values greater than the mean value of 2.7×10^{-7} shown; (c) Same as Fig. 7b but values less than the mean value of 2.7×10^{-7} shown.

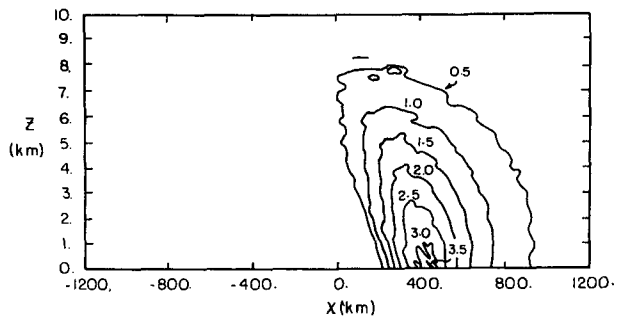

FIG. 8. Distribution of rain water (10^{-2} g kg^{-1}) in Expt. E at 22 hours.

downdraft interface is roughly 1 in 60 and that the *vertical* scale of the updraft–downdraft couplet is just a few kilometers.

The potential vorticity field (Fig. 7) in the case with rain evaporation (Expt. E) shows some interesting structure. In addition to the large condensation-generated maximum at the surface front, which also occurs in the condensation-only case (Expt. C), a secondary maximum generated by the vertical gradient of rain evaporation extends up the back side of the frontal zone. A negative anomaly of potential vorticity is produced near the surface on the back side of the front. The noise in the potential vorticity field develops as a consequence of the breakdown of the advection term in the liquid water equation close to the time of frontal collapse.

4. Summary

Evaporation of rain has been included in the moist, semigeostrophic frontogenesis model of Thorpe and Emanuel (1985). Since rain falls out of the updraft into the cold air behind the main frontal zone, its evaporation strengthens the frontal circulation and leads to faster collapse of the surface gradients. The main structural effect of evaporation is the formation of a narrow, downward-sloping downdraft (which might be termed a "cold conveyor belt" in Browning's terminology) just beneath the concentrated band of saturated ascent on the warm side of the frontal zone. Much of the total frontal circulation is now concentrated in these two zones. As the associated cross-front ageostrophic velocities of these conveyor belts are on the order of several meters per second, they should be detectable with Doppler radar.

Although we have not included effects of the ice phase in this model, several qualitative inferences can be made. In the first place, melting may be expected to increase further the frontal circulation, since it too will occur principally in the descent region. Moreover, snowflakes, as they fall more slowly, will stay in the sloping downdraft for longer periods, and evaporate faster for the same concentration of condensed water. Thus, inclusion of the ice phase may be expected to amplify the features associated with evaporation. Quantification of this effect is left for future work.

Acknowledgments. This work has been supported by a grant from the National Science Foundation, ATM-8815008. The authors would like to thank Joel Sloman for preparing the manuscript and Isabelle Kole for drafting the figures.

APPENDIX

Validity of the Geostrophic Momentum Approximation in Frontal Zones with Evaporating Rain

According to Emanuel (1985), a requirement for the validity of the geostrophic momentum approximation applied to two-dimensional fronts forced by deformation is

$$\left|\frac{dU_{ag}}{dt} - \alpha U_{ag}\right| \ll |fV'_g|, \tag{A1}$$

where U_{ag} is the ageostrophic zonal flow and V'_g is the departure of the meridional geostrophic wind from the background deformation flow.

The magnitude of the ageostrophic zonal wind associated with evaporation may be estimated by equating the magnitude of the first term in (3) with that of the last term and using (11) for S:

$$|U_{ag}| \sim \left|\frac{H}{L}\frac{g}{f^2}\frac{L_v}{C_pT}E_r\right|, \tag{A2}$$

where H and L are typical vertical and horizontal scales in geostrophic coordinates. We take as an estimate of the left-hand side of (A1)

$$\left|\frac{dU_{ag}}{dt} - \alpha U_{ag}\right| \approx \left|U_g\frac{\partial U_{ag}}{\partial X}\right| \approx \left|U_g\frac{U_{ag}}{L}\right|. \tag{A3}$$

Then (A1) becomes

$$\left|U_g\frac{U_{ag}}{L}\right| \ll |fV'_g|. \tag{A4}$$

If U_g and V'_g have the same magnitude, then (A4) may be written as a requirement on the ageostrophic Rossby number:

$$\frac{|U_{ag}|}{fL} \ll 1. \tag{A5}$$

Substituting (A2) for $|U_{ag}|$ gives a requirement on the evaporation rate:

$$E_r \ll \frac{C_pT}{L_v}\frac{L^2}{Hg}f^3 \sim 10^{-6}\ \text{s}^{-1}, \tag{A6}$$

where the numerical estimate of the right-hand side of (A6) has been made using typical values of the parameters.

For the integration described in this paper, maximum evaporation rates are about an order of magnitude smaller than this upper bound. We conclude that *for stable (nonconvective) frontal circulations, condensation is a much more severe constraint on the validity of the geostrophic momentum approximation than evaporation of rain.*

REFERENCES

Atlas, D., R. Tatehira, R. C. Srivastava, W. Marker and R. E. Carbone, 1969: Precipitation-induced mesoscale wind perturbations in the melting layer. *Quart. J. Roy. Meteor. Soc.*, **95,** 544–560.

Carbone, R., 1982: A severe winter squall line. Part I: Stormwide hydrodynamic structure. *J. Atmos. Sci.*, **39,** 258–279.

Emanuel, K. A., 1985: Frontal circulations in the presence of small moist symmetric stability. *J. Atmos. Sci.*, **42,** 1062–1071.

——, 1988: Observational evidence of slantwise convective adjustment. *Mon. Wea. Rev.*, **116,** 1805–1816.

——, M. Fantini and A. J. Thorpe, 1987: Baroclinic instability in an environment of small stability to slantwise convection. Part I: Two-dimensional models. *J. Atmos. Sci.*, **44,** 1559–1573.

Garner, S. T., 1989: Fully Lagrangian numerical solutions of unbalanced frontogenesis and frontal collapse. *J. Atmos. Sci.*, **46,** 717–739.

Hoskins, B. J., 1971: Atmospheric frontogenesis models: some solutions. *Quart. J. Roy. Meteor. Soc.*, **97,** 139–153.

——, and F. P. Bretherton, 1972: Atmospheric frontogenesis models: Mathematical formation and solution. *J. Atmos. Sci.*, **29,** 11–37.

Hsie, E.-Y., R. A. Anthes and D. Keyser, 1984: Numerical simulation of frontogenesis in a moist atmosphere. *J. Atmos. Sci.*, **41,** 2581–2594.

Keyser, D., and R. A. Anthes, 1982: The influence of planetary boundary layer physics on frontal structure in the Hoskins–Bretherton horizontal shear model. *J. Atmos. Sci.*, **39,** 1783–1802.

——, and M. A. Shapiro, 1986: A review of the structure and dynamics of upper-level frontal zones. *Mon. Wea. Rev.*, **114,** 452–499.

Klemp, J. B., and R. B. Wilhelmson, 1978: The simulation of three-dimensional convective storm dynamics. *J. Atmos. Sci.*, **35,** 1070–1096.

Oliver, V. J., and G. C. Holzworth, 1953: Some effects of the evaporation of wide-spread precipitation on the production of fronts and on changes in frontal slopes and motions. *Mon. Wea. Rev.*, **81,** 141–151.

Stewart, R. E., 1985: Precipitation types in winter storms. *Pure Appl. Geophys.*, **123,** 597–609.

Szeto, K. K., C. A. Lin and R. E. Stewart, 1988a: Mesoscale circulations forced by melting snow. Part I. *J. Atmos. Sci.*, **45,** 1629–1641.

——, R. E. Stewart and C. A. Lin, 1988b: Mesoscale circulations forced by melting snow. Part II. *J. Atmos. Sci.*, **45,** 1642–1650.

Thorpe, A. J., and C. A. Nash, 1984: Convective and boundary layer parameterizations in a diagnostic model of atmospheric fronts. *Quart. J. Roy. Meteor. Soc.*, **110,** 443–466.

——, and K. A. Emanuel, 1985: Frontogenesis in the presence of small stability to slantwise convection. *J. Atmos. Sci.*, **42,** 1809–1824.

Williams, R. T., L. C. Chou and C. J. Cornelius, 1981: Effects of condensation and surface motion on the structure of steady-state fronts. *J. Atmos. Sci.*, **38,** 2365–3376.